Metrological Traceability and Crucial Detector Characteristics for UVC Metrology in UVGI Applications

P. Sharma[1,2]*, V. K. Jaiswal[1,2], S. Saha[1,2] and D. K. Aswal[1,2]

[1]CSIR-National Physical Laboratory, Dr. K.S. Krishnan Marg, New Delhi 110012, India

[2]Academy of Scientific and Innovative Research (AcSIR), Ghaziabad 201002, India

© Metrology Society of India 2022

Abstract: Ultraviolet-C (UVC) radiation-based sanitization has globally gained enormous importance in the current COVID-19 (caused by SARS-COV-2 virus) pandemic situation. The effectiveness of radiation sanitization is quantified in terms of 'radiation dose', which in turn is derived from a radiometric parameter 'irradiance', measured using UVC radiometer. Metrological traceability of irradiance/dose measurement is essentially required for achieving requisite accuracy of measurements, and hence germicidal efficacy. In the present article, the derivation of traceability for irradiance measurement using UVC radiometer is demonstrated. The critical conditions to be considered while using detector/radiometer for measuring UVC irradiance/dose in practical conditions are elaborated, avoiding which, significant errors in the UVC irradiance/dose may arise, and hence, may compromise the performance of the Ultraviolet Germicidal Irradiation (UVGI) devices.

1. Introduction

In the current scenario of global COVID-19 pandemic, ultraviolet (UV) radiation-based disinfection procedures have gained significant momentum for mitigation of the spread of Coronavirus through exposed surface and airborne transmission [1–3]. Human-to-human spread of virus/bacteria not only occurs through direct or close contacts but also through indirect interactions like contaminated objects and surfaces [4]. In the case of Novel Coronavirus, the indirect modes contribute equally to viral transmission among humans [5]. Chemical-based sanitization is commonly recommended for disinfecting the surfaces for breaking the transmission chain [7]. Disinfectants range from common soap to chemicals like sodium hypochlorite and alcohol [6]. However, chemical disinfectants are known to be noxious for people's health and cause eye, respiratory and skin irritation or damage [7, 8]. Moreover, the contact base liquid chemical disinfectants are not suitable for sanitization of surfaces of electronic devices. Though, being in use for water disinfection for a considerable amount of time now, but in the era of the COVID-19 pandemic UV radiation has emerged as a suitable non-contact-based method for sanitization of object surfaces, especially those which cannot be immersed in liquid biocides [9, 10]. Moreover, UV sanitization is most suitable for disinfection of large areas like rooms and halls as it is known not only to disinfect the surfaces but also the ambient environment [2].

UV light is a small portion of spectrum (100–400 nm), below the visible light, which is not sensed by human eye. Based on the physical and physiological effects, UV light is further subdivided in mainly three ranges, 100–280 nm, 280–315 nm, and 315–400 nm, called UVC, UVB and UVA, respectively. The UVC band of the UV region is known to have germicidal properties and impedes the spread of infection through incapacitating microorganisms and viruses through their structural modification [11]. In this regard, the UV dose imparted to a surface, for disinfection, is of prime importance as a lower dose of UV radiation will not be able to incapacitate the viral load completely [3, 11]. UV dose is quantified through the measurement of irradiance. Irradiance is a radiometric parameter which quantifies the radiant flux irradiating a unit surface area. To ascertain germicidal nature of a UV

*Corresponding author, E-mail: sharmap2@nplindia.org

irradiation, the measurement of the irradiance becomes utmost important.

Optical detector/radiometer is, in general, used to measure irradiance. Detector is a device that produces a measurable electrical signal on being exposed to optical radiation. When radiation illuminates the active area of a detector, an electrical signal is generated, which in turn is proportional to the radiant flux incident on the detector surface or irradiance. Various types of detectors such as pyroelectric detectors, bolometers, semiconductor photodiode, phototransistors, etc., are used for radiometric measurements [12, 13]. Moreover, the majority of the commercial semiconductor-based radiometric detectors are wavelength selective. Thus, being of different types, the detectors are required to be calibrated for irradiance in the wavelength range of interest before being used for measurements. To ensure accurate measurements, unbroken chain of traceability has to be ensured through documented calibration steps. However, incorrectly calibrated detectors and measurements performed in unsuitable conditions may arise large measurements errors.

In the present article, we present the establishment of the radiometric traceability for UVC detectors for irradiance. Currently, both mercury vapor lamps and UVC LED sources are being used for Ultraviolet Germicidal Irradiation (UVGI) devices [14]. The calibration of detector, however, is strongly dependent on the spectral profile of the source. Being a traditional UV source, mercury vapor lamp was chosen to establish the traceability of irradiance. In the current communication, in addition to present the establishment of the traceability for UV measurements, we discussed the important characteristics of the detectors for measurements in practical conditions.

2. Radiation Dose, Irradiance and Spectral Irradiance

UV dose, a deciding parameter for germicidal efficacy, is related to the Irradiance (E) through the relation:

$$\text{Dose}(J/m^2) = E(W/m^2) \times \text{Time}(s) \tag{1}$$

Irradiance is defined as the radiant flux (radiant power falling normal to a surface of definite area) incident on a unit surface area. In the SI (International System) system of units, it is expressed in W/m² (watts per square meter). In other words, it is the irradiation power delivered to a unit surface area by a radiation source (Fig. 1a).

If a radiation of radiant power (called radiant flux (φ_e)) is normally incident on a detector (as shown in Fig. 1a) of active surface area, A, then the irradiance, E_e, as measured by the detector is mathematically defined as
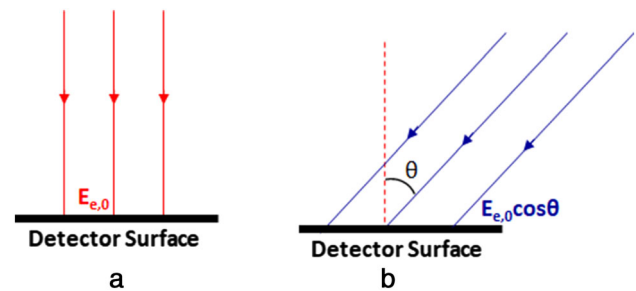

Fig. 1 Radiation incident **a** normally and **b** obliquely on a detector

$$E_{e,0} = \frac{d\varphi_e}{dA} \tag{2}$$

Instead of normal incidence, if the radiation is obliquely incident at an angle θ (Fig. 1b) then the measured irradiance is mathematically defined as

$$E_{e,\theta} = E_{e,0}\cos\theta = \frac{d\varphi_e}{dA}\cos\theta \tag{3}$$

Irradiance can be measured directly using a detector whose output parameter is calibrated against a standard incident radiant flux value. An ideal radiometric detector must show a decrease in measured irradiance by a factor of $\cos\theta$ as the incidence direction of radiation changes from normal to an oblique incidence at an angle θ, hence, should follow the cosine law. According to cosine law, irradiance measured by a detector should be directly proportional to the cosine of the angle between the direction of the incident light and the normal to the surface of the detector active area.

In the present discussion, it is important to point out that the response of the detectors is limited by the wavelength range. Hence, the irradiance measured by the detector is also affected by its spectral response. The issue of selective spectral response in radiometric detectors can be overcome by using a spectroradiometer in which irradiance is measured individually over the wavelength spectrum. This parameter of spectral irradiance can be mathematically described as

$$E_{e,\lambda} = \frac{d^2\varphi_e}{dAd\lambda}\cos\theta \tag{4}$$

The total irradiance, E_e, in the wavelength range λ_1 to λ_2 can be mathematically derived from the spectral irradiance by integrating the spectral irradiance over the wavelength λ_1 to λ_2.

$$E_e = \int_{\lambda_1}^{\lambda_2} \frac{d^2\varphi_e}{dAd\lambda}\cos\theta d\lambda \tag{5}$$

However, employing a spectroradiometer for regular measurements, especially in the field measurements, is
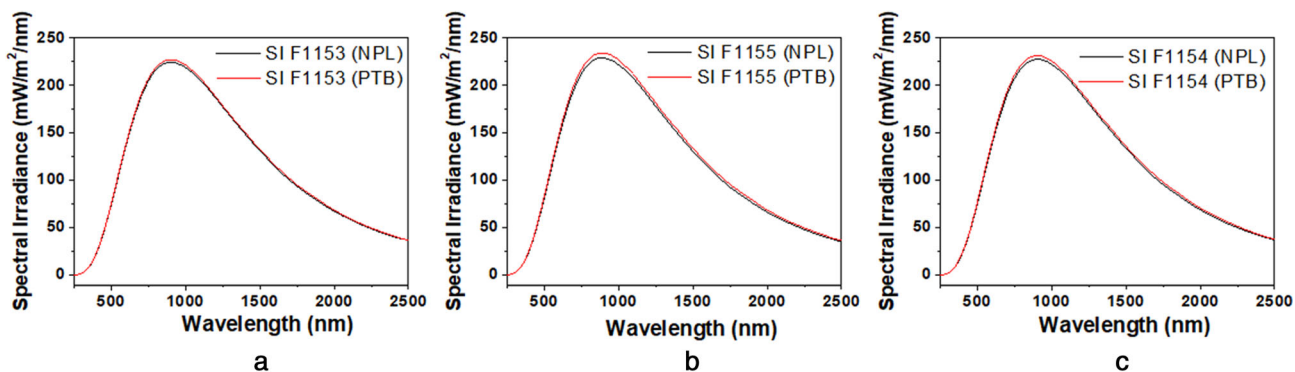
Fig. 2 Spectral irradiance of FEL type reference standard lamps recorded at a distance of 50 cm
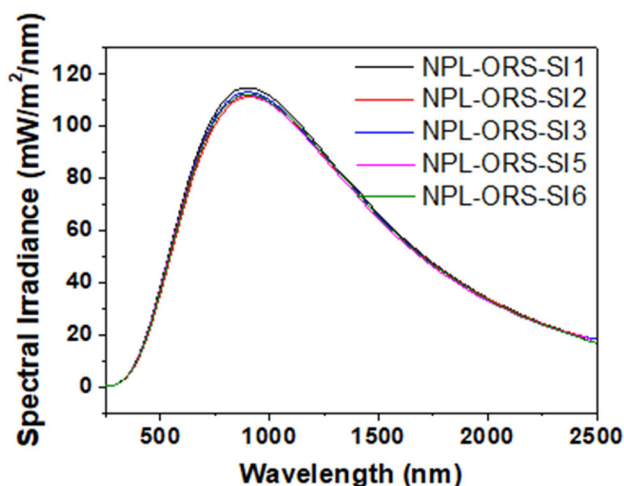

Fig. 3 Spectral irradiance of working standard lamps at a distance of 70 cm

relatively tedious, and detectors being of small size, come in handy for routine measurements.

3. Establishing Metrological Traceability of Irradiance for UVC Detector Calibration

The radiometric measurements are dependent on the measurement of irradiance, and for accurate measurements, establishment of traceability to SI (International System of Unit) is essential. National Metrology Institutes (NMIs) all over the world realize and maintain metrological traceable physical standard for various radiometric parameters like radiant flux, irradiance, radiant intensity, etc. [15–19].

Irradiance is the radiometric parameter which can be directly measured by a calibrated sensor or detector. A SI traceable calibration of detectors is even more important for their application in the measurement of UVGI as it directly impacts the well-being of the society. In radiometry, primary standards are of two types: radiation source-based primary standard and detector-based primary

standard. As the name suggests, the source-based primary standards are radiation sources based on some physical phenomenon with known radiation spectral output. Radiation sources like synchrotron and blackbody radiation sources are widely used as radiation-based primary standards [20, 21]. On the other hand, the detector-based standards are based on radiation-absorbing receivers whose temperature rises when they are exposed to radiation. They work on the principle of ESR (electrical substitution radiometry) [22] and the incident radiant power is enumerated through its comparison with an electrical power which produces the same rise in temperature. Thus, the optical power and electrical power are equated on the basis of their respective thermal effect. Cryogenic radiometer establishes the equivalence of radiation and electrical power at cryogenic temperatures and is used as standards for detector-based radiometry at various NMIs [21]. Cryogenic radiometers are used to establish detector spectral responsivity scale. Usually using a laser source or a broadband source, a cryogenic radiometer calibrates a trap detector which in turn is used to calibrate the filter radiometer. The filter radiometer transfers the measurement scale to blackbody through its temperature measurement. The blackbody spectrum is then used to establish the scale of spectral irradiance.

NPLI derives its traceability of spectral irradiance (250–2500 nm) from a set of three 1000 W (8A, 110 V) Quartz Halogen Lamps (commonly known as spectral irradiance standard FEL lamps) calibrated from leading NMIs. Presently, NPLI has set of lamps calibrated against reference standard lamps of PTB Germany in 2012, and against primary standard blackbody of NPL UK in 2018. Figure 2a–c shows the spectral irradiance values provided by PTB Germany and NPL UK, for these sets of lamps, respectively. As shown in Fig. 2, FEL lamp has comparatively low spectral irradiance values in the wavelength region 250–400 nm. The uncertainty in the spectral irradiance measurements of reference standard lamps in the
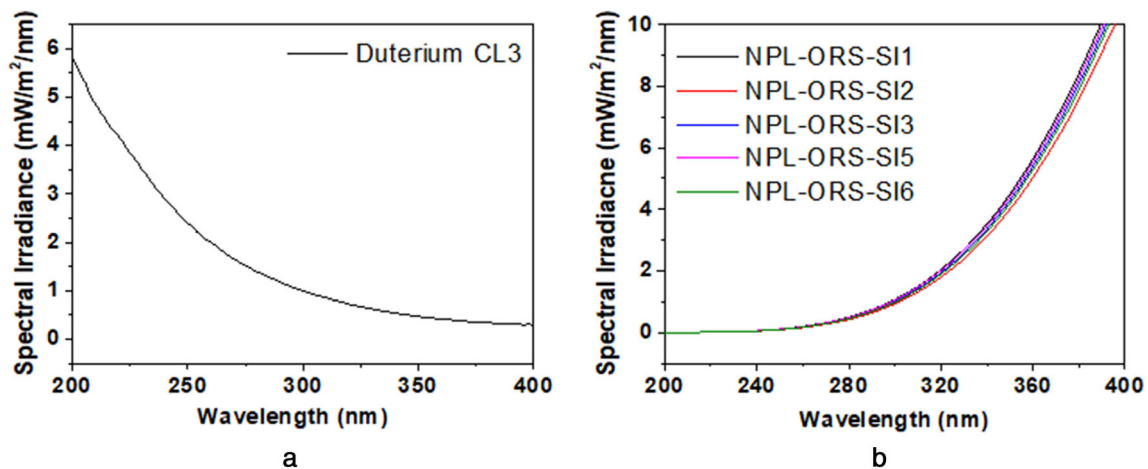
Fig. 4 **a** Spectral irradiance of CL3 lamp at a distance of 20 cm **b** Measured spectral irradiance of working standard lamps with respect to CL3 lamp at a distance of 20 cm

range of 250–400 nm, 400–800 nm, and 800–2400 nm is stated as 2.0–1.2%, 1.1%, and 1.2–6.2%, respectively.

The FEL lamps calibrated for spectral irradiance are, in turn, employed to transfer the spectral irradiance scale to a DTMs-300 Spectroradiometer (Bentham, UK) as explained in reference [23]. The DTMs-300 is a double monochromator-based spectroradiometer having three detectors spanning over a wide wavelength range of 200 nm to 3000 nm. It employs a lead sulfide detector for the infrared range, silicon photodiode for the near-infrared and visible range and photomultiplier tube for the UV range, which are automatically selected depending on the wavelength region being measured. The entrance port of the spectrometer is coupled with a 150 mm diameter PTFE-based integrating sphere. The spectroradiometer is employed to measure spectral irradiance of light sources based on the method of comparison. The spectroradiometer is first calibrated with a standard lamp of known spectral irradiance. Based on the calibration, spectral irradiance of the lamp under test is obtained from the electrical signal generated by the detectors. The initial calibration of the spectroradiometer was made using one of the reference lamps over the wavelength range 250–2500 nm.

To minimize the burning hours of reference standard lamp, the spectral irradiance scale is transferred to a set of working standard lamps. Presently, a total of five numbers of FEL lamps calibrated for spectral irradiance in the range of 250–2500 nm are used as working standards for measurement/calibration work/services. These lamps had also been previously calibrated directly against reference standard lamps of PTB Germany. The spectral irradiance curve of these lamps are shown in Fig. 3.

Due to lack of calibration values in the wavelength range 200–250 nm, these FEL lamps cannot be used directly to calibrate the UVC detector. However, a

Bentham, UK make Deuterium reference standard lamp (CL3 lamp) with substantial irradiance in the UV range of 200 nm–400 nm is suitable for calibration of the UV detector. Hence, CL3 lamp of rated electrical power 30 W with circular window is used for UV measurements.

To establish the link between spectral irradiance values of deuterium and FEL types lamps, the following procedures were adopted after taking care of observation distances. Using the known values of spectral irradiance of the CL3 lamp (Fig. 4a), the DTMs-300 Spectroradiometer was calibrated over the wavelength range of 200–400 nm. The five working FEL standard lamps, calibrated against the reference standard lamp, were then recalibrated against the CL3 lamp over the same wavelength range and their spectral irradiance values were derived. The measured spectral irradiance for the working standard lamps with the CL3 calibration are shown in Fig. 4b.

Thus, two sets of spectral irradiance data were obtained for the set of five FEL working standard lamps. One set was over the wavelength range of 250–2500 nm with respect to the reference FEL lamp, while the second set was over 200–400 nm with respect to CL3 lamp. It is evident that the obtained spectral irradiance values for the overlapping wavelength range of 250–400 nm for the set of working standard lamps were well comparable. Thus, the spectral irradiance values of the CL3 lamp were validated through an indirect traceability chain.

The CL3 lamp was further used to calibrate the DTMs-300 spectroradiometer and the spectral irradiance was measured for a 11 W mercury vapor working standard lamp (Hg-W-1). The irradiance spectrum for the Hg-W-1 mercury lamp within the wavelength range 250–260 nm is shown in Fig. 5 along with the measured signal current at a distance of 50 cm. The spectral irradiance data were used to calculate the total/integrated irradiance of Hg-W-1
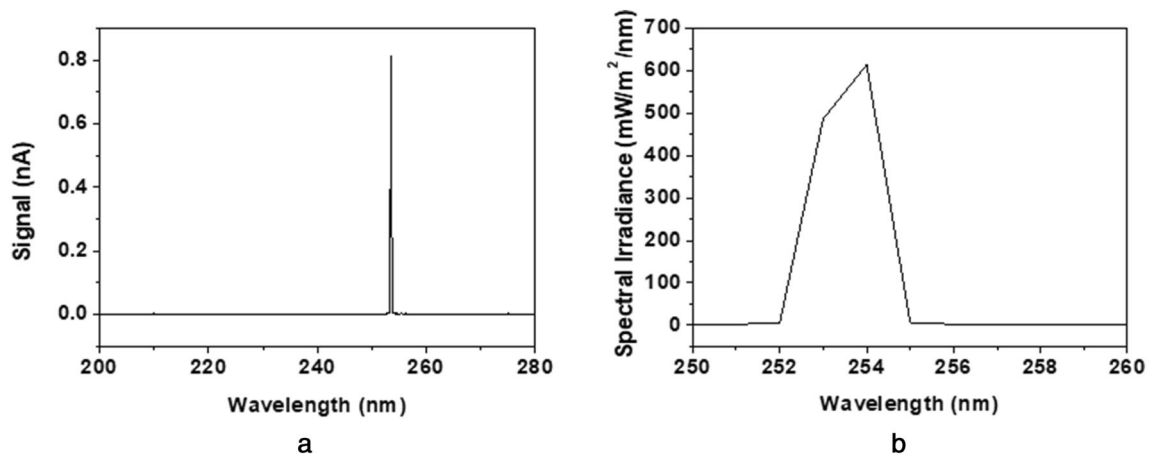
Fig. 5 a Signal and **b** Spectral Irradiance of the mercury vapor working standard lamp (Hg-W-1) recorded at a distance of 50 cm
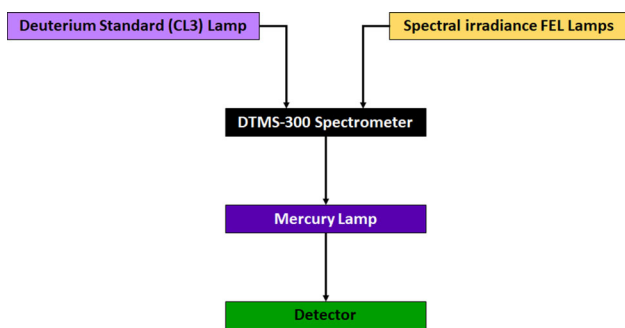

Fig. 6 Traceability scheme for UVC Detector

(*Integrated Irradiance$_{Hg-W-1}$*) in the range of 200–280 nm. The *Integrated Irradiance$_{Hg-W-1}$* was calculated to be 1.1 W/m^2 at a distance of 50 cm. The irradiance of the mercury lamp was in turn used to calibrate a PRC UVC radiometer. The mercury lamp was made to illuminate the PRC UVC detector and the photocurrent (*Photocurrent$_{Hg-W-1}$*) was recorded and thus the integrated responsivity (*Integrated Responsivity$_{PRC}$*) was obtained for the detector for the 254 nm line of Hg Source.

$$\text{Integrated Responsivity}_{PRC} = \frac{\text{Photocurrent}_{Hg-W-1}}{\text{Integrated Irradiance}_{Hg-W-1}}$$

(6)

The detector was then used to measure UVC content of the lamps under test. The photocurrent generated by the PRC detector (*Photocurrent$_{DUT}$*), on being illuminated by the lamps under test, was recorded and the irradiance was obtained as:

$$\begin{aligned}\text{Irradiance}_{DUT} = {}&(\text{Integrated Responsivity}_{PRC})^{-1}\\&\times \text{Photocurrent}_{DUT}\end{aligned}$$

(7)

Thus, the validity of measurement as well as traceability of the measured irradiance is ensured. The schematic chart of the traceability obtained for the detector is shown in Fig. 6.

4. Detector Characteristics Affecting Irradiance Measurements

Detector is a device whose output (usually electrical) is directly proportional to the radiant flux of the radiation incident normally on its active surface. Two important characteristics of a detector viz. Detector Responsivity and Cosine correction require special attention while using a detector for irradiance measurement.

4.1. Detector Responsivity

In general, responsivity is the ratio of output to input of a detector system. For a radiometric detector, responsivity quantifies the electrical output with respect to the radiometric input. Responsivity of a detector is the ratio of the current generated in response to the amount of radiometric power incident on the detector. Hence, detector responsivity is generally expressed in the unit Ampere per Watt (A/W).

Detectors are sensitive to specific spectral region. For example, the detector used in the present study is most sensitive to the UVC band of the electromagnetic spectrum. As the quantum efficiency of the detector depends on the wavelength of radiation, the detector's response is not constant over the entire wavelength range. The responsivity of the detector thus further depends on the wavelength. This variation in the responsivity with changing wavelength of incident radiation is termed as detector spectral responsivity.

The calculation of the responsivity over an extended wavelength spectrum inherently assumes a flat spectral

response of the detector as spectral variation of the detector is not considered in the calculations. For example, if a UVC detector shows a current of I Ampere on being exposed to a known radiation (spanning over certain UVC wavelength region) containing total power C W incident on the detector, then the responsivity can be calculated as I/C A/W. This value of integrated responsivity does not consider the spectral profile of detector responsivity. This may lead to serious errors in observations taken with the detector in presence of different radiation having diverse spectra.

To elucidate the concept of introduction of errors due to wavelength-selective responsivity, theoretical calculations were carried out. We considered three detectors having different spectral responsivity profiles (Fig. 7a). The spectral responsivity profile of Detector A is assumed to be an ideal, i.e., flat response between 200 and 280 nm, while that of Detector B is considered to be of a near-ideal detector. The spectral responsivity of Detector C is considered as of commercially available UVC detector. Three quasi-monochromatic UVC sources are assumed (shown in Fig. 7b) and their spectral power distribution is generated theoretically in the UVC range with FWHM of about 20 nm and peaks at 220 nm (S_1), 250 nm (S_2), and 260 nm (S_3) having same peak power. Figure 7b also depicts a source (S_4) having a peak at 220 nm, however, with lower spectral power as compared to the other sources. The wavelength peak is chosen keeping in mind the UVC line of KrCl-based Excimer source, Mercury vapor lamp, and UV LED source, respectively. The source S_1 with peak at 220 nm having larger spectral power (Fig. 7b) is considered as the calibrating source, while the other three sources (S_2, S_3 and S_4 in Fig. 7b) are taken as the test sources.

The integrated responsivity of all the three detectors (A, B and C) considering the source S_1 as the standard can be calculated using the following expression:

$$R_i(A/W) = \frac{\int R_i(\lambda)\phi_1(\lambda)d\lambda}{\int_{200}^{280}\phi_1(\lambda)d\lambda} \qquad (8)$$

where, R_i and $R_i(\lambda)$ are the integrated responsivity and spectral responsivity of given detector. $\phi_1(\lambda)$ is the spectral radiant flux, of the source S_1 used as standard for detector calibration, incident normally on the detector placed at certain distance from S_1. The calculated values of the integrated responsivities of the three detectors are shown in Table 1.

These detector responsivities can then be used to measure the radiant flux of the sources S_2 and S_3. The current produced by the given detector, I_{ph}, on being exposed to a radiation of spectral radiant flux $\phi(\lambda)$ is given by

$$I_{ph}(A) = \int_{200}^{280} R_i(\lambda)\phi(\lambda)d\lambda \qquad (9)$$

The radiant flux incident on the detector can further be calculated using the respective detector integrated responsivities calibrated using the source S_1. Thus, the amount of radiant flux (ϕ) incident on the detector can be evaluated as:

Table 1 Calculated values of the calibrated responsivities of the detectors under study

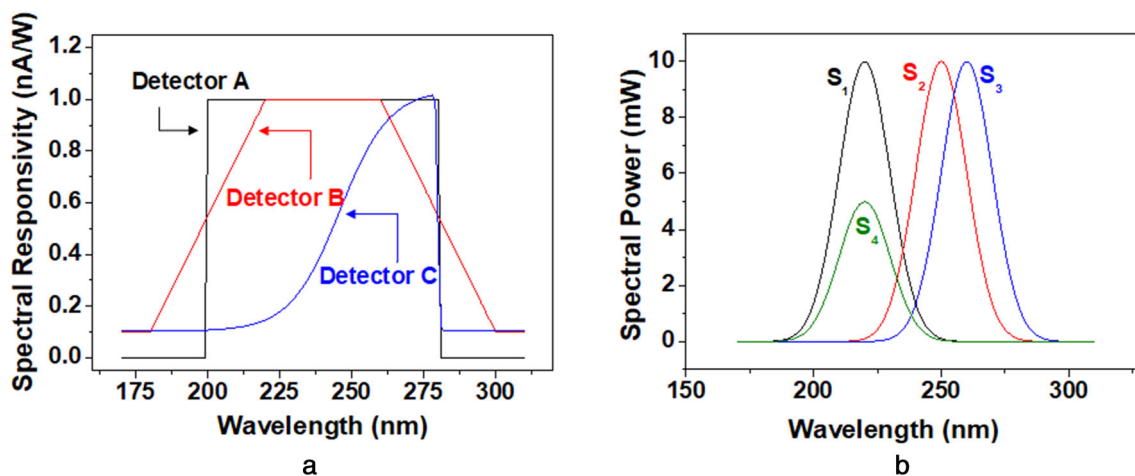| Detector	R (nA/W)
A	1.000
B	0.913
C	0.158

Fig. 7 **a** Spectral Responsivity of detectors under study **b** Spectral Power Distribution of the light sources

$$\phi(W) = \frac{I_{\mathrm{ph}}}{R_i} \tag{10}$$

Further, the irradiance E or the flux density on the surface of detector can then be obtained as:

$$E(W/m^2) = \frac{\phi}{\mathrm{DetectorArea}} \tag{11}$$

The radiant flux from the two light sources S_2 and S_3 incident on the detectors A, B and C, which are calibrated against the light source S_1, are shown in Table 2. As the detector A exhibits ideal flat response in the wavelength region 200–280 nm, the radiant flux read by the Detector A does not show any error. Further, the radiant flux read by the Detector B exhibiting near ideal response, for source S_3 gives correct value; however, for source S_2 gives error of about 8%. This is attributed due to the fact that the peaks of the calibration source S_1 and the test source S_3 are almost symmetrically placed with respect to the leading edge and the falling edge of the spectral responsivity curve of the detector B. The Detector C, which has skew-shaped spectral responsivity as exhibited by different commercially available detectors fabricated for particular type of light source, shows error in reading the radiant flux of more than 300% and 400% for the sources S_2 and S_3, respectively. However, for the test source S_4 with peak at 220 nm having smaller irradiance, the radiant flux read by all the three detectors show good correspondence with the actual radiant flux of the source. This is due to the fact that the calibrating source of the detectors and the test source have similar spectrum.

Thus, it can be inferred that the detectors with flat response (like Detector A) provide correct measurement irrespective of the calibration source, test source or their spectra. However, as we deviate toward a non-ideal flat spectral responsivity, the spectrum of the calibrating source and test source start playing role in the measurements. The near-ideal detector (Detector B) shows error depending on the source, while the real detector (Detector C) shows a large error for both the measurements owing to a difference in the spectrum of the calibrating and test sources. Further, on measuring a test source having a similar spectrum as that of the calibrating source, all the three detectors confirm to the actual value of radiant flux. The results clearly indicate that for correct measurements the calibration of the detectors should be carried out using a source having a similar spectrum as that of the test source.

As, in general, the detectors, especially UVC detectors, do not have a flat spectral response, the integrated responsivity is specific for a source and cannot be used to measure UVC irradiance for any other type of sources. The detector would require calibration with a source which has a similar spectrum as that of the lamp under test [24]. It is important to note the fact that calibration is 'not only calibration but calibration according to the specific application.'

However, in practical situations, measurements may be required to be made for sources whose spectrum is absolutely different from that of the source used for calibration. In such a situation a mathematical correction may be applied to correct the measured irradiance by modifying the formula for calculating spectral mismatch. It is evident from Table 2 that the detector A would not show any error due to spectral mismatch of the calibrating source and the source under test. However, the measurements with detector C show considerable error for sources with different spectral profiles. A measurement value correction factor f may be applied which corrects the measured irradiance for mismatch in the spectrum of the calibrating and the measured source [25]. The correction factor f can be calculated as:

$$f = \frac{\int\limits_{200}^{280} R_{i\mathrm{Rel}}(\lambda)\phi_{1\mathrm{Rel}}(\lambda)d\lambda}{\int\limits_{200}^{280} \phi_{1\mathrm{Rel}}(\lambda)d\lambda} \bigg/ \frac{\int\limits_{200}^{280} R_{i\mathrm{Rel}}(\lambda)\phi_{j\mathrm{Rel}}(\lambda)d\lambda}{\int\limits_{200}^{280} \phi_{j\mathrm{Rel}}(\lambda)d\lambda} \tag{12}$$

where, $R_{i\mathrm{Rel}}(\lambda)$ is the spectral responsivity of given detector. $\phi_{1\mathrm{Rel}}(\lambda)$ is the normalized spectral radiant flux of the calibrating standard source S_1, while $\phi_{j\mathrm{Rel}}(\lambda)$ is the normalized spectral radiant flux of the source being measured. The correction factor calculated for the measurements using detector C is presented in Table 3.

It may be observed that the factor f corrects the measured flux and hence an accurate measure of irradiance can be obtained if the relative detector spectral responsivity, and relative spectra of the calibration and the measurand source are known.

Table 2 Theoretical power and measured power of the test sources (all the detectors are calibrated with calibration source S_1)

	Test source S_2	Test source S_3	Test source S_4
Actual calculated Radiant flux value	250.63 mW	249.52 mW	124.76 mW
Radiant flux considering detector A	250.63 mW (error: 0%)	249.52 mW (error: 0%)	124.76 mW (error: 0%)
Radiant flux considering detector B	270.13 mW (error: 7.78%)	249.52 mW (error: 0%)	124.76 mW (error: 0.00001%)
Radiant flux considering detector C	1037.76 mW (error: 314.06%)	1273.19 mW (error: 458.73%)	124.76 mW (error: 0.0001%)

Table 3 Theoretical power and measured power (using detector C) of the test sources with and without correction factor f (the detector C is calibrated with calibration source S_1)

	Test source S_2	Test source S_3	Test source S_4
Actual calculated Radiant flux value	250.63 mW	249.52 mW	124.76 mW
Radiant flux considering detector C	1037.76 mW (error: 314.06%)	1273.19 mW (error: 458.73%)	124.76 mW (error: 0.0001%)
Correction factor (f)	0.2407	0.1955	1
Corrected radiant flux considering detector C	249.79 mW (error: 0.34%)	248.91 mW (error: 0.24%)	124.76 mW (error: 0.0001%)

4.2. Cosine Correction of Detectors for UV Measurement

During calibration of detectors, the UV-radiation is normally incident on the detector placed at a significant distance to fulfill inverse square law, and hence, cosine errors of detector don't influence results. However, in the large number of practical scenarios, especially in UV sanitization boxes, radiations at any point inside the box are incident from all the directions and hence, cover broad angles. In these cases, the cosine correction of the detector becomes very important to measure irradiance accurately. According to the cosine law, irradiance at any sectional area is directly proportional to the cosine of the angle between the direction of the incident light and the normal to the sectional area. Hence, for radiometric measurements, cosine correctors are attached in front of sensors. A detector with a poor cosine response gives a lower value of irradiance for oblique incidence, which may mislead evaluating the correct dose requirement for UVGI disinfection.

Figure 8 shows three detectors having different cosine responses (P, Q and R). The P curve (red) represents a perfect cosine response, while the Q (green) and R (blue) curves are that of a typical poorer cosine response of detector, R one being inferior to the Q. In case of normal incidence there is no difference in reading of the detectors (point A in Fig. 8). However, on being irradiated with a radiation at an angle θ, the detector with cosine responses P and R shows a difference of $\varepsilon_{\cos\theta}$ (points B_1 and B_2 in Fig. 8) in the measurements. Thus, a detector with a poor cosine response records a lower irradiance value.

To expound the effect of cosine correction on irradiance measurements, we consider a cubical box of length, breadth and height of 55 cm (Fig. 9). An isotropic radiation point source is considered to be placed at the center of the top face. We assume to place three detectors in various positions, placed one at a time, on the bottom face and measure the irradiance. One of the detectors has a perfect cosine correction (P), while the other two detectors have been assumed to have a poor cosine response (Q and R) with a cosine error of $f_2 = 7\%$ (Q) and $f_2 = 36\%$ (R).

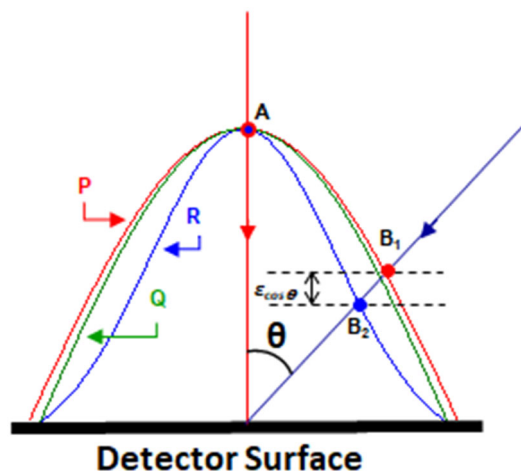Figure 10 shows the relative difference between the irradiance measurements of the detectors with perfect

Fig. 8 Measurement affected by cosine response of detectors (P curve shows a perfect cosine response, while the Q and R curves depict typical detectors of poorer cosine response)
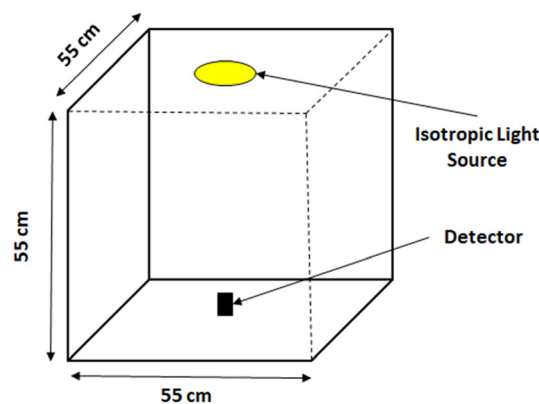

Fig. 9 Schematic diagram of the enclosure assumed for calculation

cosine response and those with $f_2 = 36\%$ (Fig. 10a) and $f_2 = 7\%$ (Fig. 10b). It can be observed that, though the errors are quite lesser at places closer to points of normal incidence, while error of almost 25% creeps in the measurements at the corners of the enclosure for detector with f_2 error of 36%. However, this error falls below to 2% value with a detector having f_2 error of 7%. It is important to mention that the height of the assumed cubical box plays
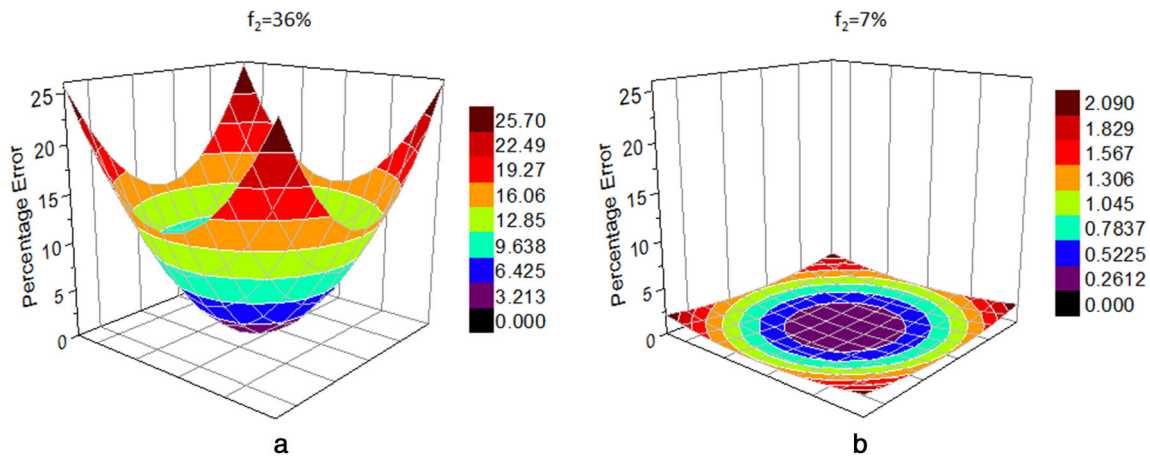
Fig. 10 Relative irradiance measurement error for the detectors having poor cosine response (a: f_2 error = 36% b: f_2 error = 7%) with respect to the detector having perfect cosine response

a major role in the error, which increases with decrement in the height of the enclosure.

In field/application measurements, it is not always possible to ensure normal incidence. Hence, while making UV measurements it is of utmost importance to warrant that the detector has an adequate cosine corrector to ensure the reliability of the irradiance measurement, which in turn confirms estimation of correct dose of radiation thus avoiding adverse implication of inadequate UVGI treatment.

5. Uncertainty in UVC Irradiance Measurement

Uncertainty evaluation is an integral part of any measurements or calibrations. The actual uncertainty in calibration largely depends on the method of calibration, measurement set-up and standards used [24]. The uncertainty can be evaluated by the method recommended by the JCGM [26].

The detector-based traceability for UVC measurement can be provided through calibration of test detectors against a standard UV lamp (Hg-W-1) in our case which derives its traceability from a Deuterium reference standard lamp (CL3 lamp). On the other hand, the calibration of UVC source is provided by its spectral calibration against the CL3 lamp through the standard spectroradiometer.

A schematic diagram of the setup for calibration of the Hg-W-1 lamp is shown in Fig. 11. A similar setup is used to calibrate any UVC lamp for disseminating traceability to the user. The calibration uncertainty of the CL3 lamp is 5.2% at a coverage factor of $k = 2$. The typical uncertainty in transferring the calibration to the Hg-W-1 lamp is about 2.86% which is calculated as per standard budget published elsewhere [23].
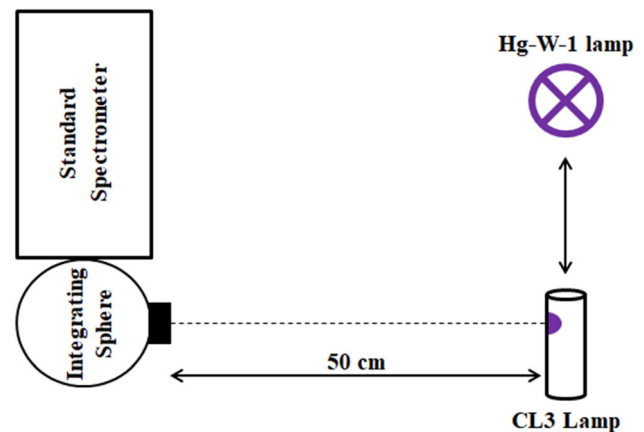

Fig. 11 Schematic diagram of the setup for calibration of Hg-W-1 lamp

The integrating sphere in the setup plays the role of a diffuser and ensures an angularly and spatially uniform radiation input to the monochromator. Integrating sphere produces illumination with uniform irradiance, by multiple reflection from a diffused surface, for the entry port of the monochromator due to the fact that the solid angle projected from any point on sphere surface to any area element of the sphere remains the same, regardless of location. The exit port of the sphere couples this uniform illumination with the monochromator [27]. Thus, the input to the monochromator depends on the imaging of the exit port on the input of the monochromator. Hence, imaging of the exit port becomes a source of uncertainty in measurements being carried out using integrating sphere. The image of the exit port on the monochromator input, in turn, depends on the spatial and spectral properties of the illumination sources. In the current calibration setup, the measurements are made at a distance of 70 cm which is fairly large as compared to the dimension of the light-emitting window of

the calibration and the test light sources. This combined with the fact that the windows for light throughput are kept similar for the two sources causes the calibration source and the test source to behave as a nearly point source. The other factor affecting the imaging of the output port on the monochromator slit is the spectral mismatch of the two sources. In the calibration setup, a PTFE-based integrating sphere has been used. Owing to the flat reflectance of PTFE in the UV region the imaging of the output port of the sphere will not be affected substantially due to spectral mismatch of the calibration and test sources [28]. The spectral measurements carried out for the calibration of Hg-W-1 lamp further reduce the effect of the spectral mismatch of the sources on the imaging of the output port of the sphere on the monochromator input. Further, in the present work, the calibration is performed on relative scale with respect to the standard lamp without intermittent realignment or change in the setup. Hence, the sources of uncertainty relating to the setup (like alignment, and geometry) will be correlated and spectrally flat [29]. Hence, the uncertainties in measurements due to spatial and spectral mismatch of the sources in the present calibration setup are quite small in comparison to other sources of uncertainties. However, it is important to point out that this factor requires consideration when extended sources are used for calibration.

A typical uncertainty budget for the lamp calibration is shown in Table 4. It is important to point out that the calibration of the reference standard lamp is a major contributor to the uncertainty. The uncertainty in the calibration of the Hg-W-1 lamp comes out to be 5.93% at a coverage factor of $k = 2$. A test UVC source from the user may be calibrated in the same way but the uncertainty may vary depending on the stability of the lamp under test.

The test detectors requiring calibration are measured against the calibrated working standard, i.e., the Hg-W-1 lamp. A schematic diagram of the calibration setup is
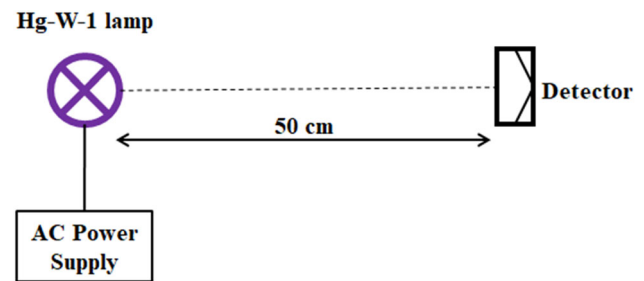

Fig. 12 Schematic diagram of the setup for calibration of test detector against calibrated lamp

shown in Fig. 12. The main sources of uncertainty to be considered by a testing laboratory are as follows:

- Uncertainty in irradiance of the working standard lamp due to its calibration (Type *B*)
- Uncertainty due to stability of UV radiation from the working standard lamp (Type *A*)
- Uncertainty due to stability of the test detector (Type *A*)
- Uncertainty due to reproducibility of the test detector (Type *B*)
- Uncertainty in position of the test detector with respect to the working standard (Type *B*)
- Uncertainty due to optical alignment of the detector (Type *B*)

Apart from the mentioned sources, uncertainty in measurement is also caused by variations in the electrical input to the working standard. Moreover, environmental factors like temperature and humidity are known to cause changes in spectral responsivity of UV detectors [30]. Additionally, the optical components of the detector are prone to degradation due to exposure to UV radiation [30]. The contributions from these factors are very small and hence not included. A typical uncertainty budget for detector calibration is shown in Table 5. The detector calibration in

Table 4 Typical uncertainty budget for calibration of Hg-W-1 lamp

Uncertainty sources	Relative standard uncertainty (%)	Relative contribution (%)
Uncertainty in calibration of reference standard lamp	2.6	76.8
Uncertainty in distance of reference standard lamp	0.04	0.02
Uncertainty in distance of working standard lamp	0.04	0.02
Uncertainty in alignment of reference standard lamp	0.8	7.3
Uncertainty in alignment of working standard lamp	0.8	7.3
Uncertainty in stability of standard spectrometer	0.12	0.2
Uncertainty in stability of reference standard lamp	0.5	2.8
Uncertainty in stability of working standard lamp	0.5	2.8
Uncertainty in reproducibility of working standard lamp	0.5	2.8
Expanded uncertainty ($k = 2$)	5.93%	

Table 5 Typical uncertainty budget for calibration of test detector against calibrated lamp

| Uncertainty sources	Relative standard uncertainty (%)	Relative contribution (%)
Uncertainty in irradiance of working standard lamp	2.97	71.49
Uncertainty due to stability of working standard lamp	0.5	2.03
Uncertainty due to detector repeatability	1.0	8.12
Uncertainty due to detector reproducibility	1.5	18.27
Uncertainty in position of detectors	0.04	0.01
Uncertainty due to alignment of the detector	0.1	0.08
Expanded uncertainty ($k = 2$)	7.02%	
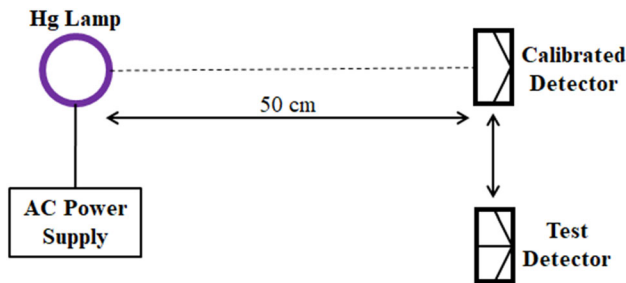
Fig. 13 Schematic diagram of the setup for calibration of test detector against calibrated detector

the current setup has an uncertainty of 7.02% at a coverage factor of $k = 2$.

The detectors calibrated at CSIR-NPL can be used by the testing laboratories for further dissemination of traceability for UVC measurement. The detectors calibrated by the above method are used as reference standards against which the test detectors from the users can be further calibrated. A schematic diagram of a typical setup for calibrating test detectors against a reference detector is shown in Fig. 13. The major sources of uncertainty to be considered by a testing laboratory carrying out detector calibrations against a standard detector are as follows:

- Uncertainty in responsivity of the detector due to its calibration (Type *B*)
- Uncertainty due to stability of the calibrated detector (Type *A*)
- Uncertainty due to stability of the UV lamp used in the setup (Type *A*)
- Uncertainty due to stability of the test detector (Type *A*)
- Uncertainty due to reproducibility of the test detector (Type *B*)
- Uncertainty in position of standard detector (Type *B*)
- Uncertainty in position of test detector (Type *B*)
- Uncertainty due to optical alignment of the standard detector (Type *B*)
- Uncertainty due to optical alignment of the test detector (Type *B*)

Here, it is important to point out that the detector-based calibration should be carried out using a similar source (mercury vapor lamp in the present discussion), as used in calibration of the standard detector. Use of different UVC sources will lead to errors due to spectral mismatch [24, 31]. A typical uncertainty budget for calibration of a test detector against a calibrated detector is shown in Table 6. The test detector calibration has an uncertainty of 8.21% at a coverage factor of $k = 2$.

Table 6 Typical uncertainty budget for calibration of test detector against calibrated detector

Uncertainty sources	Relative standard uncertainty (%)	Relative contribution (%)
Uncertainty in responsivity of calibrated detector	3.51	73.1
Uncertainty due to stability of calibrated detector	1.0	5.9
Uncertainty due to stability of UV lamp	0.5	1.5
Uncertainty due to repeatability of test detector	1.0	5.9
Uncertainty due to reproducibility of test detector	1.5	13.4
Uncertainty in position of standard detector	0.04	0.01
Uncertainty in position of test detector	0.04	0.01
Uncertainty due to alignment of the calibrated detector	0.1	0.06
Uncertainty due to alignment of the test detector	0.1	0.06
Expanded uncertainty ($k = 2$)	8.21%	

6. Conclusion

Considering the increasing demand for accurate UVC measurements for UVGI applications during the current pandemic period, a traceability chain for UVC irradiance measurements using radiometer was established. The UVC irradiance of a mercury vapor lamp was measured using double monochromator-based spectroradiometer, calibrated against FEL type spectral irradiance reference standard lamps and deuterium lamp in UVC spectral band. UVC radiometer was then calibrated against low-pressure mercury vapor lamp, emitting prominent characteristic line at 254 nm in UVC band. The study clearly highlighted the important fact that the detector should be calibrated against the source of similar spectral profile for which it is expected to be used. Further, crucial characteristics of the detector, namely spectral responsivity and cosine response, and their role in irradiance measurement, especially in application conditions, were briefly illustrated with qualitative study. It was also demonstrated that only calibration is not sufficient to ensure correct measurements. Even calibrated detectors having poor cosine response may give erratic measurements in various measurement conditions. Thus, good detector characteristics are also among the few crucial requirements of correct measurements other than its calibration and, therefore, require attention before dissemination of scale of measurement.

References

[1] ISO 15714:2019 Method of evaluating the UV dose to airborne microorganisms transiting in-duct ultraviolet germicidal irradiation devices, Hosted by International Organization for Standardization (ISO) website. https://www.iso.org/obp/ui/#iso:std:iso:15714:ed-1:v1:en. Accessed 02 January, 2021.

[2] M. Bentancor and S. Vidal, Programmable and low-cost ultraviolet room disinfection device. HardwareX, 4 (2018) e00046.

[3] C.S. Heilingloh, U.W. Aufderhorst, L. Schipper, U. Dittmer, O. Witzke, D. Yang, X. Zheng, K. Sutter, M. Trilling, M. Alt, E. Steinmann and A. Krawczyk, Susceptibility of SARS-CoV-2 to UV irradiation. Am. J. Infect. Control, 48 (2020) 1273–1275.

[4] L. Fiorillo, G. Cervino, M. Matarese, C. D'Amico, G. Surace, V. Paduano, M.T. Fiorillo, A. Moschella, A.L. Bruna, G.L. Romano, R. Laudicella, S. Baldari and M. Cicciù, COVID-19 surface persistence: a recent data summary and its importance for medical and dental settings. Int. J. Environ. Res. Public Health, 17 (2020) 3132.

[5] R. Karia, I. Gupta, H. Khandait, A. Yadav and A. Yadav, COVID-19 and its modes of transmission. SN Comprehen. Clin. Med., 2 (2020) 1798–1801.

[6] M.H. Al-Sayah, Chemical disinfectants of COVID-19: an overview. J. Water Health, 18 (2020) 843–848.

[7] J.-H. Ahn, K.-H. Eum, Y.-K. Kim, S.-W. Oh, Y.-J. Kim and M. Lee, Assessment of the dermal and ocular irritation potential of alcohol hand sanitizers containing aloe vera with in vitro and in vivo methods, Molecular & cellular. Toxicology, 6 (2010) 397–404.

[8] J.L.J. Jing, T.P. Yi, R.J.C. Bose, J.R. McCarthy, N. Tharmalingam and T. Madheswaran, Hand sanitizers: a review on formulation aspects, adverse effects, and regulations, international journal of environaental research and public. Health, 14 (2020) 3326.

[9] M.C. Collivignarelli, A. Abbà, I. Benigna, S. Sorlini and V. Torretta, Overview of the main disinfection processes for wastewater and drinking water treatment plants. Sustainability, 10 (2018) 86.

[10] A. Guridi, E. Sevillano, IDl. Fuente, E. Mateo, E. Eraso and G. Quindós, Disinfectant activity of A portable ultraviolet C equipment. Int. J. Environ. Res. Public Health, 16 (2019) 4747.

[11] M. Heßling, K. Hönes, P. Vatter and C. Lingenfelder, Ultraviolet irradiation doses for coronavirus inactivation—review and analysis of coronavirus photoinactivation studies, GMS Hyg. Inf. Control, 15 (2020) Doc08.

[12] A.S. Morris and R. Langari, Measurement and instrumentation: theory and application. Elsevier, London (2016).

[13] G. Hyseni, N. Caka and K. Hyseni, Infrared thermal detectors parameters: semiconductor bolometers versus pyroelectrics. WSEAS Trans. Circuits Syst., 9 (2010) 238–247.

[14] A. E. Torres, A. B. Lyons, I. Kohli, A. Parks-Miller, D. Ozog, I. H. Hamzavi and H. W. Lim (2020) Ultraviolet-C and other methods of decontamination of filtering facepiece N-95 respirators during the COVID-19 pandemic 19: 746.

[15] Optical Measurement, NPL UK, Hosted by NPL, UK website. https://www.npl.co.uk/products-services/optical-measurement. Accessed 19 December, 2020.

[16] The National Laboratory for Photometry and Radiometry, Hosted by RISE, Sweden website. https://www.ri.se/en/what-we-do/expertises/national-laboratory-photometry-and-radiometry. Accessed 19 December, 2020.

[17] Optical Radiation Group, Hosted by NIST, USA website. https://www.nist.gov/pml/sensor-science/optical-radiation. Accessed 19 December, 2020.

[18] Photometry and radiometry, Hosted by PTB, Germany website. https://www.ptb.de/cms/en/research-development/subject-areas-in-metrology/photometry-and-radiometry.html. Accessed 19 December, 2020.

[19] Optical Radiation Standards, Hosted by CSIR-NPL, India website. https://www.nplindia.in/optical-radiation-standards. Accessed 19 December, 2020.

[20] R. Müller, A. Hoehl, R. Klein, G. Ulm, M. Abo-Bakr, K. Bürkmann-Gehrlein, J. Feikes, M. V. Hartrott, J. S. Lee, J. Rahn, U. Schade and G. Wüstefeld, Coherent Synchrotron Radiation at the Metrology Light Source, In: Proceedings of EPAC08, Genoa, Italy (2008).

[21] S. Saha, V.K. Jaiswal, P. Sharma and D.K. Aswal, Evolution of SI base unit candela: quantifying the light perception of human eye. MAPAN-J. Metrol. Soc. India, 35 (2020) 563–573.

[22] Ö. Bazkir and F. Samedov, Electrical substitution cryogenic radiometer based spectral responsivity scale between 250–2500 nm wavelengths. Opt. Appl., 34 (2004) 427–438.

[23] P. Sharma, V.K. Jaiswal, Sudama, R. Mehrotra and H.C. Kandpal, Up-gradation of a spectral irradiance measurement facility at National Physical Laboratory India. MAPAN-J. Metrol. Soc. India, 25 (2010) 21–28.

[24] G. Xu and X. Huang, Calibration of broadband UV radiometers—methodology and uncertainty evaluation. Metrologia, 40 (2003) S21–S24.

[25] A. Gugg-Helminger, CIE 220:2016—characterization and calibration method of UV radiometers. IUVA News, 19 (2017) 19–24.

[26] Evaluation of Measurement Data—Guide to the Expression of Uncertainty in Measurement, Joint Committee for Guides in Metrology (JCGM), 2008 (JCGM 100:2008).

[27] A.V. Arecchi, T. Messadi and R.J. Koshel, Field guide to illumination. SPIE Press, Washington (2007).

[28] V.R. Weidner, J.J. Hsia and B. Adams, Laboratory intercomparison study of pressed polytetrafluoroethylene powder reflectance standards. Appl. Opt., *24* (1985) 2225–2230.

[29] P. Saunders, E. Woolliams, H. Yoon, A. Todd, M. Sadli, E. v. d. Ham, K. Anhalt, L. Werner, D. R. Taubert, S. Briaudeau and B. Khlevnoy, Uncertainty estimation in primary radiometric temperature measurement (2018), *Hosted by BIPM website*. https://www.bipm.org/documents/20126/2619564/MeP-K-2018_Absolute_Primary_Radiometry_Uncertainty.pdf/

b9a9ea9a-8de2-3da4-0eb9-4d0b534782f0 Accessed 24 November, 2021.

[30] T.C. Larason and C.L. Cromer, Sources of error in UV radiation measurements. J. Res. Natl. Inst. Stand. Technol., *106* (2001) 649–656.

[31] G. Xu and X. Huang, Characterization and calibration of broadband ultraviolet radiometers. Metrologia, *37* (2000) 235–242.